

# A smoothing monotonic convergent optimal control algorithm for NMR pulse sequence design

Ivan I. Maximov\* and Niels Chr. Nielsen†

*Centre for Insoluble Protein Structures (inSPIN),*

*Interdisciplinary Nanoscience Centre (iNANO) and Department of Chemistry,*

*University of Aarhus, Langelandsgade 140, DK-8000 Aarhus C, Denmark*

Julien Salomon and Gabriel Turinici‡

*CEREMADE, Universite Paris Dauphine, Place de Marechal de Lattre de Tassigny, 75775 Paris Cedex 16, France*

(Dated: October 23, 2018)

The past decade has demonstrated increasing interests in using optimal control based methods within coherent quantum controllable systems. The versatility of such methods has been demonstrated with particular elegance within nuclear magnetic resonance (NMR) where natural separation between coherent and dissipative spin dynamics processes has enabled coherent quantum control over long periods of time to shape the experiment to almost ideal adoption to the spin system and external manipulations. This has led to new design principles as well as powerful new experimental methods within magnetic resonance imaging, liquid-state and solid-state NMR spectroscopy. For this development to continue and expand, it is crucially important to constantly improve the underlying numerical algorithms to provide numerical solutions which are optimally compatible with implementation on current instrumentation and at same time are numerically stable and offer fast monotonic convergence towards the target. Addressing such aims, we here present a smoothing monotonically convergent algorithm for pulse sequence design in magnetic resonance which with improved optimization stability lead to smooth pulse sequence easier to implement experimentally and potentially understand within the analytical framework of modern NMR spectroscopy.

---

\* Present address: Institute of Neuroscience and Medicine (INM-4), Research Centre Jülich GmbH, 52425 Germany

† ncn@inano.dk

‡ Gabriel.Turinici@dauphine.fr

## I. INTRODUCTION

Optimal control theory (OCT) is a powerful method for control and design of processes within quantum dynamics. Originally the method was applied for problems within engineering and economics.[1, 2] During the past decade or so, optimal-control-based methods have been increasingly used for a development of new experiments within optical spectroscopy,[3–8] quantum information processing, [9–14] liquid- and solid-state nuclear magnetic resonance (NMR) spectroscopy, [15–29] magnetic resonance imaging (MRI),[30–36] and dynamic nuclear polarization (DNP) hybrids between electron and nuclear magnetic resonance.[37–40] Such applications have not only been useful for the specific disciplines taking advantage of new efficient design procedures and improved experimental methods, but it has also stimulated mathematical investigations in quantum optimal control theory.[41–47] The latter addresses fundamental questions concerned with controllability, convergence, and the establishment of powerful numerical methods for optimal control in quantum systems.

So far, the vast majority of optimal control applications within magnetic resonance have taken advantage of gradient-based methods, such as the gradient ascent pulse engineering (GRAPE) algorithm introduced for NMR applications by Khaneja and coworkers, [19] and recently further developed and distributed for general use by Nielsen and coworkers in an optimal control version[21, 29] of the open-source NMR simulation software SIMPSON.[48, 49] In combination with conjugated gradient algorithms, this method [19, 21, 24, 29] proves to be very powerful, as demonstrated by numerous applications in which NMR methods with improved experimental sensitivity, robustness towards variations in instrumental or spin system parameters, reduction of the undesirable effects from dissipative processes (i.e., relaxation), and experiments with lower radio-frequency (rf) power requirements and thereby reduced risks for sample heating have been developed. More recently, it has been demonstrated [38] that a monotonic convergent variant of optimal control method based on the algorithms of Krotov [2–4, 6] represents an interesting alternative to the gradient-based approaches for efficient experiment design. Our initial work with this algorithm, in a density operator formulation, exposed important computational properties of optimal control methods such as global extremum searching, fast convergence, algorithmic simplicity, and independence on time discretization in terms of convergence.

Despite increasing use, it is apparent that current methods face serious challenges in the practical realization which needs to be addressed to exploit the full potential of optimal control based methods for design of optimal experiments. This applies not least for the most challenging purposes involving large spin systems, optimizations ensuring broadband or band-selective operation with respect to certain spin system parameters (e.g., chemical shifts), and powder samples in solid-state NMR spectroscopy. For example, looking at the many optimal control pulse sequences proposed so far,

it appears that many of these display quite wild oscillations in phase and amplitude of the rf control fields (see, e.g., Refs.[18, 20–29]) which may complicate implementation on available instrumentation with limitations on the speed and accuracy of phase and amplitude switching. Furthermore, it turns out that GRAPE displays a quite strong dependence on the initial guess of the pulse sequence, dependence on the applied time discretization (i.e., the number of pulse variables, and their duration), as well as unpredictable convergence to local extremum points. Along the same lines, the monotonic Krotov-based algorithm faces problems with numerical instability and difficulties in a selection of parameters controlling the flow of operations and balance of necessary running costs.[38] These problems have introduced undesired needs for intuition, experience, and repetition of optimizations with a very large set of different initial guesses in the usage of these methods as replacement for stronger mathematical recipes. Although part of these problems have been overpassed in recent adoptions for wave function formalism in optical spectroscopy,[44] a strong need for solutions to the problems still exists for magnetic resonance applications typically performed within a density operator formalism.

In this paper, we present a modified monotonic algorithm which stabilizes convergence and smooths the resulting NMR pulses sequences through the use of a frequency truncation technique in course of the optimization. The latter aspect is practically important realizing that most optimal control sequences presented so far within NMR spectroscopy display quite significant and fast amplitude and phase modulations, which may cause unnecessary problems upon implementation on available spectrometer hardware. This work builds on related techniques introduced in the field of the laser control of alignment and rotation [50] for an unique controlling field.

## II. THE OPTIMAL CONTROL PROBLEM

The most typical setup for optimal control pulse sequence design in NMR spectroscopy involves systematic generation of optimal radio-frequency (rf) pulse sequences which in a given spin system either (i) accomplish the most efficient transfer of coherence or polarization from a given initial spin state  $\rho_0$  to a desired target spin state  $C$  (often referred to as state-to-state transfer) or (ii) synthesize a specific effective (or average) Hamiltonian[51, 52] emphasizing or suppressing certain parts of the internal nuclear spin interactions to tailor the Hamiltonian for evolution under desired interactions. These interactions may provide a desired state-to-state coherence/polarization transfer, specific information, or provide spectral simplification, e.g., in the form of improved spectral resolution.

In absence of dissipative processes, the dynamics of the nuclear spin system may be described by the Liouville-von

Neumann equation

$$\frac{d\rho(t)}{dt} = -i[H(t), \rho(t)], \quad (1)$$

where  $\rho(t)$  is the density matrix (initial state:  $\rho(0) = \rho_0$ ) and  $H(t)$  is a Hamiltonian of the spin system. In the high-field approximation, the latter takes the form

$$H(t) = H_0 + \sum_k \omega_k(t) H_k, \quad (2)$$

with the first term collecting all internal nuclear spin interactions (chemical shifts as well as  $J$ , dipole-dipole, and quadrupole couplings) and the latter describing external rf manipulations with the amplitude  $\omega_k(t)$  (in angular frequency units) for the spin operator  $H_k$  (typically  $H_k = I_x, I_y, S_x, S_y$  for an I-S two-spin system) being our control fields. The solution to the equation of motion in Eq. (1) is typically expressed as

$$\rho(t) = U(t)\rho_0U^\dagger(t), \quad (3)$$

where the unitary operator (or propagator)  $U(t) = \hat{D} \exp\left(-i \int_0^t H(t') dt'\right)$  links the unitary evolution with the Hamiltonian in Eq. (2).  $\hat{D}$  is the so-called Dyson time-ordering operator.

Optimal control relies on optimization of a functional of the type

$$J_i(\omega) = \phi_i - \sum_k \lambda_k \int_0^T \omega_k^2(t) dt, \quad (4)$$

with the first term denoting the final cost (or the objective) and the latter term the running cost considering the collected energy/power used to reach the optimum. The influence of the running cost is scaled by a so-called penalty factor  $\lambda_k$  (which may be constant, as assumed here, or time-dependent if, e.g., specific rise and fall time behaviour of the pulses are desired). This convex running cost improves the convergence of the optimization methods. Furthermore, it facilitates development of pulse sequences without too excessive rf power consumption.

For state-to-state transfers between Hermitian operators  $C$  and  $\rho_0$ , the final cost (i.e., the overall transfer efficiency) may be expressed as

$$\phi_1 = \text{Tr}(C\rho(T)), \quad (5)$$

where  $T$  is the overall duration of the experiment. For transfers between non-Hermitian operators the final cost may be formulated as [29, 38]

$$\phi_2 = |\text{Tr}(C^\dagger\rho(T))|^2. \quad (6)$$

For synthesis of a desired propagator  $U_D$ , the final cost is given by

$$\phi_3 = \text{Re} \left[ \text{Tr}(U(T)U_D^\dagger) \right]. \quad (7)$$

We note that the objectives  $\phi_i$  given above is by no means exclusive, and other variants for the target functions may be used. For example, instead of Eq.(7) one may use the squared expression  $\phi'_3 = |\text{Tr}(U_D^\dagger U(T))|^2$ . The preferential form of the target function typically depends strongly on the given optimization problem. [15, 19, 24, 28, 29]

### III. MONOTONIC CONVERGENCE

The aim of optimal control experiment design is for a given period of time  $T$  and a given time discretization (i.e., number of pulses, typically taken equidistantly over the time  $T$ ) to find rf control fields (i.e.,  $\omega_k(t)$ ) which lead to the maximum of the functional in Eq. (4). The Krotov-based monotonic algorithms accomplish this using a Lagrange approach with an adjoint propagator  $B(t)$ , or a Lagrange multiplier for an unconstrained functional as described in Ref. ([38]), using a combination of forward propagation with  $U(t)$  (Eq.(3) ) and backward propagation using a conjugated equation for  $B(t)$ . We note that different formulations exist for such calculations, including that of Tannor and coworkers [3] closely following the original formulations of Krotov, a different variant by Zhu et al. [4], and a more general approach (embracing the methods of Tannor and Zhu) as described by Maday et al.[6] in context of waveforms and Maximov et al.[38] in context of density operators. For simplicity, we here restrict to the original Krotov approach as formulated by Tannor et al.[3] (corresponding to  $\delta = 1$  and  $\eta = 0$  in Refs. ([6]) and ([38])), while noting that the more general formulation with arbitrary  $\delta$  and  $\eta$  parameters may readily be implemented at the expense of slightly more complicated formulas.

A prerequisite for monotonic convergence is that the target operator  $C$  is positive semi-definite. While this condition is obviously fulfilled for optimization of effective Hamiltonians, it will, for example, for optimization of transfer between Hermitian operators require the final cost function to be modified to  $\tilde{\phi} = \phi + \kappa \text{Tr} (U(T)U^\dagger(T))$  as proposed previously.[38]

The proof for monotonic convergence, in the case of Hermitian operators, may readily be established considering the following decomposition of the variation in the cost functional values between arbitrary rf pulses controls  $\omega$  and

$\omega'$  (in a discrete representation):

$$\begin{aligned}
J(\omega') - J(\omega) &= \text{Tr} \left( (U'_N - U_N)(U_N^\dagger - U'_N) \right) + \text{Tr} \left( C(U'_N - U_N)\rho_0(U_N^\dagger - U'_N) \right) \\
&+ 2 \sum_{j=2}^{N+1} \text{Re} \left[ \text{Tr} \left\{ \left( e^{i\Delta t \sum_k \omega_{k,j-1} H_k} e^{-i\Delta t \sum_k \omega'_{k,j-1} H_k} - E \right) AU'_{j-1} B_{j-1} A^\dagger \right\} \right] \\
&- \Delta t \lambda \sum_k (\omega'_{k,j-1} - \omega_{k,j-1})(\omega'_{k,j-1} + \omega_{k,j-1}),
\end{aligned} \tag{8}$$

where we have applied the second-order Strang method to evolve the propagator  $U_j$  and the Lagrange multiplier  $B_j$ . [44] The time step  $\Delta t$  is defined through the number of bins  $N$  and the overall time  $T = N\Delta t$ , while the matrix exponent  $A$  is defined as  $A = e^{-0.5i\Delta t H_0}$ .  $E$  is the identity operator. We assume all functions to be constant during the time step  $\Delta t$  rendering computation of the matrix exponents straightforward.

The discrete set of propagators ( $U_j$ ) and Lagrange multipliers ( $B_j$ ) may be obtained using the following equations

$$\begin{aligned}
U_{j+1} &= A e^{-i\Delta t \sum_k \omega_{kj} H_k} A U_j, \\
U_0 &= E,
\end{aligned} \tag{9}$$

$$\begin{aligned}
B_j &= B_{j+1} A e^{-i\Delta t \sum_k \omega_{kj} H_k} A, \\
B_N &= \Theta(C),
\end{aligned} \tag{10}$$

with the operator  $\Theta(C)$  defined by Eqs. (5)–(7) and the desired efficiency. For example, for Hermitian state-to-state transfer

$$\Theta(C) = \kappa U_N + C U_N \rho_0, \tag{11}$$

where  $\kappa$  is an insignificant scaling factor. [38]

To ensure positiveness of the functional difference  $J(\omega') - J(\omega)$  at each time step, we need to maximize the last string of Eq.(8). Following the approach previously described for wave functions, [44] it appears convenient to re-express the two last terms of Eq.(8) as a function  $f_j(\omega'_j)$  depending on a vector variable  $\omega'_j$  of dimension  $k$  relating to the time step  $j$ ,

$$\begin{aligned}
f_j(\omega'_j) &= 2\text{Re} \left[ \text{Tr} \left\{ \left( e^{i\Delta t \sum_k \omega_{k,j-1} H_k} e^{-i\Delta t \sum_k \omega'_{k,j-1} H_k} - E \right) AU'_{j-1} B_{j-1} A^\dagger \right\} \right] \\
&- \Delta t \lambda \sum_k (\omega'_{k,j-1} - \omega_{k,j-1})(\omega'_{k,j-1} + \omega_{k,j-1}).
\end{aligned} \tag{12}$$

In this formulation, the updated control fields  $\omega'_{k,j}$  should be found locally (in time) through a minimization problem of dimension  $k$  for the vector function  $-f_j(\omega'_j)$  (corresponding to maximization of  $f_j(\omega'_j)$  and the corresponding functional in Eq.(8)), which due to the non-commutative relationships of the operators  $H_k$  in the matrix exponents

can not straightforwardly be simplified further.[6, 44] The minimization may be conducted starting with an appropriate initial guess, using routines such as conjugated gradients or quasi-Newton.[53] The iteration equation for the rf controls  $\omega'_j$  may be expressed as

$$\omega_j^{new} = \arg \min_{\omega'_j} \{-f_j(\omega'_j)\}, \quad (13)$$

with the rf fields  $\omega_j$  from a previous iteration step used as an initial guess for the minimization problem Eq.(13).

Equation (13) guarantees monotonic convergence of the functional  $J(\omega)$  for all time steps in each iteration step through solution of an unconstrained nonlinear optimization problem. Indeed,  $f_j(\omega'_j = \omega_j) = 0$ , so that  $-f(\omega_j^{new}) \leq 0$ . In other words, there exist a pulse sequence  $\omega_j^{new}$  such that  $J(\omega_j^{new}) \leq J(\omega_j)$ . Moreover, note that if the algorithm finds that  $J(\omega_j^{new}) = J(\omega_j)$  then every local optimization procedure has failed to find a strictly better control. In this case, a local maximum has been found. Note also that the previous approach is independent of the optimization method used in the local optimization problems in Eq.(13).

#### IV. FREQUENCY CONSTRAINING AND SMOOTHING

Direct application of the monotonic algorithm outlined above, as well as previous gradient-based algorithms, often lead to optimal pulse sequences with significant oscillations in the rf field amplitudes and phases. [18, 20, 23, 25, 29, 38, 40] These variations not only hamper analytical understanding of the function of optimal pulse sequences but may also complicate practical implementation on available instrumentation. To stimulate generation of smoother solutions, we here demonstrate that the optimal control algorithms may be combined with standard frequency truncation techniques with a regularization substep that retains monotonic convergence.

Given  $\omega$ , an arbitrary control, suppose that a better control  $\omega^{new}$  has been obtained, i.e.  $J(\omega) < J(\omega^{new})$ . A way to define a smoother improving control  $\omega^{smooth}$  is to consider an interpolation between  $\omega^{new}$  (i.e., those typically displaying significant oscillations) and a regularized version of it (cf. Ref. [50]). In this way define for all  $k$

$$\omega_k^{smooth} = (1 - \alpha)\omega_k^{new} + \alpha\mathbb{F}(\omega_k^{new}), \quad (14)$$

where  $\alpha$  is a regularization parameter and  $\mathbb{F}(\omega)$  defines the frequency truncation. The frequency truncation may be accomplished in many ways, e.g., using built-in functions in MATLAB [62] or simply by Fourier transforming the pulse sequence, removing high-frequency components, and transforming it back to the time domain using an inverse Fourier transformation.

Following the proofs in the previous section, it is obvious that  $\alpha = 0$  ensure monotonic behaviour and thereby  $J(\omega_{\alpha=0}^{\text{smooth}}) \geq J(\omega)$ . The same is almost true when  $\alpha \rightarrow 0$  as well. Accordingly, an iterative sub-algorithm may be established which generates a smooth and monotonic solution:

1. start from  $\alpha = 1$ ;
2. test  $J(\omega^{\text{smooth}}) \geq J(\omega)$ ?
3. if not, decrease  $\alpha$ , for example, halving the value and go to step 2.

With this ingredient and the formula in Eqs. (9) - (11), we can formulate the overall algorithm. Consider a parameter  $Tol > 0$ .

1. Set the initial random guess  $\omega^0 = (\omega_{j,k}^0); j = 1, \dots, N; k > 0$ .
  2. Compute the corresponding state  $U_0$  and  $B_0$  according to Eqs. (9)-(10).
  3. Set  $\epsilon = +\infty, \ell = 0$ .
  4. While  $\epsilon > Tol$  do
    - a. Do forward propagation and search new rf field  $\tilde{\omega}^{\ell+1}$  according to the procedure in Sec. III
    - b. Apply the frequency truncation sub-algorithm with regularization to find  $\alpha^\ell$  that preserves the monotonicity, i.e.:  $J((1 - \alpha^\ell)\tilde{\omega}^{\ell+1} + \alpha^\ell F(\tilde{\omega}^{\ell+1})) \geq J(\omega^\ell)$
    - c. Define  $\omega^{\ell+1} = (1 - \alpha^\ell)\tilde{\omega}^{\ell+1} + \alpha^\ell F(\tilde{\omega}^{\ell+1})$
    - d. Set  $\epsilon = J(\omega^{\ell+1}) - J(\omega^\ell)$
    - e. Do backward propagation to compute  $B^{\ell+1}$  the solution of Eq. (10) with  $\omega = \omega^{\ell+1}$
    - f. Do  $\ell = \ell + 1$
- End While.

It is important to note that frequency truncation technique with regularization could equally well be applied to other known optimal control approaches, such as GRAPE and different variants of Krotov-based optimal control.

## V. DESIGN OF SMOOTH NMR EXPERIMENTS

While the overall applicability of optimal control for NMR experiment design has been demonstrated and verified numerically and experimentally in numerous previous papers,[15–17, 19–22, 24, 26–29] we will demonstrate numerically



in this paper the implication of our smoothing procedure and monotonic convergence in optimal control design of a set of simple NMR experiments. We address specifically spin-state selective, non-Hermitian coherence transfer through  $J$  couplings for liquid-state NMR applications and excitation of the central transition of  $^{23}\text{Na}$  for applications in magnetic resonance imaging (MRI). Lists containing rf amplitudes and phases for the optimal control pulse sequences as well as Matlab scripts used to generate these can be found in Supplementary Material.[63]

### A. Coherence-order and spin-state-selective coherence transfer

For a two-spin,  $J$ -coupled spin systems in the context of liquid-state NMR, the internal Hamiltonian may in the high-field approximation be cast as

$$H_0 = \pi J 2 I_z S_z, \quad (15)$$

where  $I_z$  or  $S_z$  represent  $z$ -components of the spin operators for the  $I$  and  $S$  spins in the present example coupled through a scalar coupling of size  $J = 140$  Hz. To exemplify transfer between non-Hermitian operators, we assume the initial state to be represented by +1-quantum coherence on the  $S$  spin (i.e.,  $\rho_0 = S^+$ ) and to further demonstrate spin-state-selective transfer,[54–57] we assume that the destination operator is -1-quantum coherence on the  $I$  spin with the  $S$  spin being in the  $\alpha$ -state corresponding to only one of the lines in the  $J$ -coupled doublet excite (i.e.,  $C = I^- S^\alpha$ ).

In this case of transfer between non-Hermitian operators, we use the target function in Eq.(6) modified to ensure our target being positive semi-definite. This leads to the modified objective  $\tilde{\phi}$  and the operator  $\Theta(C)$ :

$$\tilde{\phi} = \phi_2 + \text{Tr}(U(T)U^\dagger(T)), \quad (16)$$

$$\begin{aligned} \Theta(C) = & U^\dagger(T) + \rho_0 U^\dagger(T) C^\dagger \text{Tr} \left[ U^\dagger(T) \rho_0^\dagger U(T) C \right] \\ & + C^\dagger U^\dagger \rho_0 \text{Tr} \left[ U(T) \rho_0 U^\dagger(T) C^\dagger \right], \end{aligned} \quad (17)$$

where we, relative to the expression in Eq. (11), assumed the scaling factor to be  $\kappa \equiv 1$  for the sake of simplicity. Our control fields are represented by the amplitudes (angular frequencies)  $\omega_k(t)$  of  $x$ - and  $y$ - phase rf irradiation on the spins  $I$  (operators  $I_x$  ( $k=1$ ) and  $I_y$  ( $k=2$ )) and  $S$  (operators  $S_x$  ( $k=3$ ) and  $S_y$  ( $k=4$ )). According to unitary bounds on spin dynamics,[58, 59] the maximum achievable transfer efficiency in this case is 1. For the optimizations we set the excitation period to  $T = 7.14$  ms (corresponding to  $1/J$ ) and the number of pulses to  $N = 200$ .

Addressing this specific optimization problem, Figure 1 compares pulse sequences (i.e.,  $I$  and  $S$  spin rf field strengths) obtained on basis of a random initial pulse sequence using the gradient-based optimal control algorithm

GRAPE,[19] the monotonic Krotov-based optimal control algorithm of Maximov et al.,[38] and the latter combined with smoothing as described in this paper. It is quite evident that the pulse sequences developed using the two former methods display quite significant oscillations, for which the appearance depends very much on the specific optimization. In the present case it looks like the GRAPE algorithm produces a more smooth, albeit still oscillating a lot in the "waves", pulse sequence than the Krotov-based algorithm. Slight variation in parameters, such as the number of steps in the waves, may radically change this picture and in a later example we will see the opposite picture. The same variability will be seen upon inspection of the many optimal control NMR pulse sequences presented in literature so far. What is clear, however, is that the Krotov-based algorithm (as selected in this paper, but it could just as well be GRAPE) combined with frequency-truncation smoothing leads to much smoother sequences which may easier be analysed analytically and which put less demands on the spectrometer hardware upon practical implementation. Apart from this the sequences display only relatively modest variations with respect to rf power consumption (root-mean-square (RMS) average rf powers (I and S spin values separated by /) of 141/71 Hz for GRAPE, 92/91 Hz for Krotov, and 12/102 Hz for smoothing Krotov) and are essentially identical with respect to coherence transfer efficiency (99% of the theoretical maximum for all methods).

While rigid statements on the optimization speed and convergence require a much more thorough analysis (to be presented elsewhere), examples like the one in Fig. 1 provide the following crude estimate. Smooth Krotov is computation-speed wise quite similar to GRAPE, while the original Krotov approach is somewhat faster (in the order of a factor 3-5, although this number highly depends on the specific optimization). Out of 1000 optimizations based on random initial pulse sequences only 80-90 % of the GRAPE and Krotov optimizations led to sequences with more than 90% of the nominal transfer efficiency, while all sequences in this specific case passed this limit for the smooth Krotov approach. The great benefit of smooth Krotov is that it provides smooth pulse sequences, and the benefit of both Krotov variants is that they enable optimization with much more coarse time discretization (longer and fewer pulses) than the GRAPE algorithm due to its fundamentally different optimization strategy.

Figure 2 gives snapshots of pulse sequences throughout optimization using the smoothing Krotov-based optimal control algorithm starting out from a random pulse sequence (with maximum amplitude of 100 Hz). The snapshots illustrate gradual adoption of the optimal sequence to a smooth appearance. It is evident that already after 5 iterations, the control fields on the  $I$  spin almost vanishes, leaving the major action to the  $S$  spin control fields for the remaining optimization into the final pulse sequence. The final pulse sequence have quite low rf-power consumption, due to the reducing effect of the running cost ( $\lambda_1 = 10^{-4} \text{ s}^2\text{rad}^{-2}$ ,  $\lambda_2 = \lambda_1$  for both the  $I$  and  $S$  spins), and the rf

fields vary smoothly as an effect of the smoothing algorithm. The progress of the cost function and its constituents (the overall functional (cost), the transfer efficiency, and the running cost (penalty)) throughout the optimization is illustrated in Fig. 3 which also provide a numerical demonstration of monotonic convergence. It is evident that the functional converges to a value which, when considering the subtractive term from the running cost, is equal to or close to the theoretical limit after a number of iterations where the efficiency (final cost) and penalty (running cost) have displayed some exchanging oscillations before converge to the optimal values.

### B. Optimal control for satellite and central transition excitation in $^{23}\text{Na}$ MRI

Optimal control mediated experiment design is by no means restricted to spin-1/2 nuclei or systems of these. Many challenging optimization examples may be found for NMR spectroscopy or MRI in concern of quadrupolar nuclei, as recently demonstrated by optimal control pulse sequences for improved multiple-quantum magic-angle-spinning NMR[60] and for selective excitation of the central transition of  $^{23}\text{Na}$  (spin  $I = 3/2$ ) in presence of residual quadrupole couplings for magnetic resonance imaging purposes.[34–36] The latter application may be very important for  $^{23}\text{Na}$  MRI of, e.g., cartilage where the sodium concentration may be considered a reporter for disorders and degradation.[34, 61] In such applications, the ability to separate  $^{23}\text{Na}$  ions with large and very small (vanishing) residual quadrupolar couplings is regarded important as they represent different populations of relevant ions.

In this section, we demonstrate the use of the smoothing Krotov-based optimal control algorithm to design pulse sequences which selective excites the central transition  $(-\frac{1}{2}, \frac{1}{2})$  or the satellite  $(-\frac{3}{2}, -\frac{1}{2})$  or  $(\frac{1}{2}, \frac{3}{2})$  transitions of  $^{23}\text{Na}$  ions characterized by a residual quadrupole coupling frequency of  $\omega_Q/2\pi = 60$  Hz. In this case the size of the quadrupole coupling and the rf irradiation fields are comparable (often referred to as the intermediate regime) implying that experiment design by standard analytical means is not straightforward.

The optimization involves the secular, high-field-approximated first-order Hamiltonian

$$H = \frac{\omega_Q}{2}(3I_z^2 - I(I + 1)) + \omega_1(t)I_x + \omega_2(t)I_y, \quad (18)$$

where  $\omega_Q$  is quadrupole coupling frequency while  $\omega_1(t)$  and  $\omega_2(t)$  are control rf fields corresponding to the spin operators  $I_x$  and  $I_y$ , respectively (all frequencies in angular units). The nature of the optimization will be a standard state-to-state transfer with the final cost expressed by Eq. (5) with the destination operator  $C$  representing  $x$ -phase coherence on either the central transition or the satellite transitions. The initial state corresponds to the thermal equilibrium  $\rho_0 = I_z$ .

Figure 4 illustrates the performance of optimal control pulse sequences designed to enhance the central transition (in this case leading to efficient suppression of the satellite transitions although not requested in the cost function used for the optimization) or excite the satellite transitions while suppressing the central transition (also here the suppression was not specified in the cost function) relative to a hard (infinitely strong)  $90^\circ$  pulse exciting both types of transitions. The simulated spectra clearly reveal that (i) the central-transition selective excitation optimal control sequence offers a sensitivity enhancement, relative to standard single-pulse excitation, by the maximal factor of 1.5 as discussed previously by Jerschow and coworkers,[32] while ensuring reasonable suppression of the satellite transitions and (ii) the pulse sequence designed to suppress the central transition lead to satellites with unaltered intensity while the central transition is almost removed.

The optimal control pulse sequences providing selective excitation of the central transition and the satellite transitions are shown in Figs. 5A and 5B, respectively. The sequences have a overall length of  $2.25/f_Q$  (with the peak splitting  $f_Q$  related to the quadrupole coupling as  $f_Q = 3\omega_Q/2\pi$ ) and accommodates 200 pulses of equal length. The central transition excitation pulse sequence is characterized by a RMS average rf power of 45 Hz and excites the central transition with an efficiency of 99% and the satellites have been suppressed to an efficiency of 1.4% (percentages relative to the theoretical maximum). The satellite transition sequence is characterized by an RMS rf power of 54 Hz, with the satellites excited with an efficiency of 99% and the central transition suppressed 72%.

It is clear from both sequences that the optimal pulse sequence is found in the regime  $\omega_{rf} \sim \omega_Q$  for which experiment design by standard analytical means is exceedingly difficult. It is also evident that the smoothing algorithm used during optimization leads to smooth sequences offering easier implementation on conventional MRI instrumentation, than the corresponding sequences we obtained using previous optimal control formulations. The latter aspect is demonstrated in Fig. 6A by central transition-selective excitation sequences (corresponding to Fig. 5A) obtained using GRAPE or in Fig. 6B using our previous Krotov-based optimal control software. The latter pulse sequences involved 500 pulses for GRAPE and 200 pulses for the Krotov-based approach to facilitate comparison with the pulse sequences earlier proposed by Jerschow and coworkers [34] for GRAPE. In the present implementation, the GRAPE-derived sequence displays much wilder oscillations than the Krotov-based sequence.

### C. Broadband optimization

In practical applications of optimal control theory for experiment design, it is often desirable to optimize the pulse sequences to be robust toward variation in one or more spin system parameters, introducing the concepts of broadband

or bandselective excitation as described previously in the context of GRAPE [24] and Krotov-based [38] methods. Such requests may readily be incorporated into our optimal control algorithm through a modified cost function

$$J(\omega) = \kappa \text{Tr}(U(T)U^\dagger(T)) + \sum_i \text{Tr}(C^\dagger U_i(T)\rho_0 U_i^\dagger(T)) - \lambda \sum_k \int_0^T \omega_k^2(t) dt, \quad (19)$$

where each propagator  $U_i(T)$  corresponds to a specific condition, such as different chemical shifts, couplings, or orientations of the sample relative to the magnetic field (in solid-state NMR), where  $U$  is a common propagator of the system. The additional targets in the functional Eq. (19) corresponding to the broadband extension demands a modification of the condition of a monotonic convergence and as consequence changing the form of Eq.(12). This leads to a modification of the target function  $f_j(\omega'_j)$  in Eq.(12) where the part involving propagators and Lagrange matrices should be replaced by a summation

$$\dots \sum_{\text{conditions } i} A_i U'_{i,j-1} B_{i,j-1} A_i^\dagger \dots \quad (20)$$

with the propagator  $U_i$  and adjoint matrix  $B_i$  computed for each individual condition when the pulse sequence  $\omega_k$  is the same for all propagators.

To demonstrate the application of broadband optimization, we repeat our optimization of  $^{23}\text{Na}$  MRI central transition enhancement experiments for a range of quadrupole coupling around  $\omega_Q/2\pi = 60$  Hz with a deviation of  $\pm 20$  Hz. This leads to a pulse sequence with a central transition excitation profile as function of the quadrupole coupling frequency as illustrated in Fig. 7, revealing very good excitation in proximity of  $\omega_Q/2\pi = 60$  Hz as requested in the optimization. We note that it is obviously possible to specify specific regions of excitation and no excitations by entering additional conditions in the target function and algorithm.

## VI. CONCLUSION

In conclusion, we have presented a smoothing monotonically convergent optimal control algorithm for efficient design of pulse sequences for magnetic resonance applications. The proposed frequency-truncation algorithm has been incorporated into a Krotov-based optimal control procedure and demonstrated for a few of NMR examples where it leads to much smoother optimal pulse sequences than obtained using previous methods. We note that previous methods may eventually lead to smooth sequence by themselves, in particular for simple optimizations

without inhomogeneities and broadband performance request and in cases where educated guesses are present to initiate the optimization. However, in the most general case optimal control typically leads to pulse sequences with significant oscillations in phase and amplitude. In such cases our new algorithm offers a remedy to incorporate smoothness in the optimization. The smooth sequences improves the possibilities for obtaining theoretical insight for the optimal sequences and facilitates implementation on typical spectrometer hardware. We anticipate that the methods will find widespread applications for design of experiments within liquid- and solid-state NMR spectroscopy, MRI, and dynamic nuclear polarization.

### ACKNOWLEDGMENTS

This work was supported by the EU 6th Framework Program in terms of the BIODNP research infrastructure project. Support from the Danish National Research Foundation, the Danish Centre for Scientific Computing, and the Kavli Institute for Theoretical Physics, University of California, Santa Barbara (NCN) is acknowledged. GT and JS were partially supported by the “Agence Nationale de la Recherche” (ANR), Projet Blanc C-QUID number BLAN-3-139579. We thank Christoffer Laustsen for discussion on  $^{23}\text{Na}$  MRI.

- 
- [1] L. Pontryagin, B. Boltyanskii, R. Gamkrelidze, and E. Mishchenko, *The mathematical theory of optimal processes*, Wiley Interscience, New York, 1962.
- [2] V.F. Krotov, *Global methods in optimal control theory*, Marcel Dekker, Inc., New York - Basel - Hong Kong, 1995.
- [3] D. J. Tannor, V. Kazakov, and V. Orlov, in "Time-Dependent Quantum Molecular Dynamics", edited by J. Broeckhove and L. Lathouwers, Plenum, New York, 1992.
- [4] W. Zhu and H. Rabitz, *J. Chem. Phys.* **109**, 385 (1998).
- [5] H. Rabitz, R. de Vivie-Riedle, M. Motzkus and K. Kompa, *Science* **288**, 831 (2000).
- [6] Y. Maday and G. Turinici, *J. Chem. Phys.* **118**, 8191 (2003).
- [7] Y. Ohtsuki, G. Turinici, and H. Rabitz, *J. Chem. Phys.* **120**, 5509 (2004).
- [8] J. Salomon and G. Turinici, *J. Chem. Phys.* **124**, 074102 (2006).
- [9] C.M. Tesch, L. Kurtz, and R. de Vivie-Riedle, *Chem. Phys. Lett.* **343**, 633 (2001).
- [10] N. Khaneja, S.J. Glaser, and R. Brockett, *Phys. Rev. A* **65**, 032301 (2002).
- [11] J.P. Palao and R. Kosloff, *Phys. Rev. Lett.* **89**, 188301 (2002).
- [12] U. Troppmann and R. de Vivie-Riedle, *J. Chem. Phys.* **122**, 154105 (2005).
- [13] H. Jirari and W. Pötz, *Phys. Rev. A* **74**, 022306 (2006).
- [14] C. Altafini, *Quant. Inform. Proc.* **6**, 9 (2006).
- [15] S.J. Glaser, T. Schulte-Herbrüggen, M. Sieveking, O. Schedletsky, N.C. Nielsen, O.W. Sørensen, and C. Griesinger, *Science* **280**, 421 (1998).
- [16] T. Reiss, N. Khaneja, and S. J. Glaser, *J. Magn. Reson.* **154**, 192 (2002).
- [17] N. Khaneja, T. Reiss, B. Luy, and S. J. Glaser, *J. Magn. Reson.* **162**, 311 (2003).
- [18] T.E. Skinner, T.O. Reiss, B. Luy, N. Khaneja, S.J. Glaser, *J. Magn. Reson.* **163**, 8 (2003).
- [19] N. Khaneja, T. Reiss, C. Kehlet, T. Schulte-Herbrüggen, and S.J. Glaser, *J. Magn. Reson.* **172**, 296 (2005).
- [20] K. Kobzar, B. Luy, N. Khaneja, and S. J. Glaser, *J. Magn. Reson.* **173**, 229 (2005).
- [21] C.T. Kehlet, A.C. Sivertsen, M. Bjerring, T.O. Reiss, N. Khaneja, S.J. Glaser, and N.C. Nielsen, *J. Am. Chem. Soc.* **126**, 10202 (2004).
- [22] T. Vosegaard, C.T. Kehlet, N. Khaneja, S.J. Glaser, and N.C. Nielsen, *J. Am. Chem. Soc.* **127**, 13768 (2005).
- [23] B. Luy, K. Kobzar, T.E. Skinner, N. Khaneja, S.J. Glaser, *J. Magn. Reson.* **176** 179 (2005).
- [24] Z. Tošner, S.J. Glaser, N. Khaneja, and N.C. Nielsen, *J. Chem. Phys.* **125**, 184502 (2006).
- [25] T.E. Skinner, K. Kobzar, B. Luy, M.R. Bendall, W. Bermel, N. Khaneja, S.J. Glaser, *J. Magn. Reson.* **179** 241 (2006).

- [26] C. Kehlet, M. Bjerring, A.C. Sivertsen, T. Kristensen, J.J. Enghild, S.J. Glaser, N. Khaneja, and N.C. Nielsen, *J. Magn. Reson.* **188**, 216 (2007).
- [27] J. Ø. Hansen, C. Kehlet, M. Bjerring, T. Vosegaard, S.J. Glaser, N. Khaneja, and N.C. Nielsen, *Chem. Phys. Lett.* **447**, 154 (2007).
- [28] N.C. Nielsen, C. Kehlet, S.J. Glaser, and N. Khaneja, *Encyclopedia of Magnetic Resonance*, in press (2009).
- [29] Z. Tošner, T. Vosegaard, C. Kehlet, N. Khaneja, S.J. Glaser, and N.C. Nielsen, *J. Magn. Reson.* **197**, 120 (2009).
- [30] E.T. Lebsack and S.M. Wright, *IEEE Trans. Biomed. Engin.* **49**, 41 (2002).
- [31] J.L. Ulloa, M. Guarini, A. Guesalaga, and P. Irarrazaval, *IEEE Trans. Medical Imaging* **23**, 1445 (2004).
- [32] D. Xu, K.F. King, Y. Zhu, G.C. McKinnon, and Z.P. Liang, *Magn. Reson. Medicine* **59**, 547 (2008).
- [33] C.K. Anand, S.J. Stoyan, and T. Terlaky, *Proceedings of Modeling, simulation and optimization of complex processes Conference* (Hanoi, Vietnam, 2008).
- [34] J.-S. Lee, R.R. Regatte and A. Jerschow, *J. Chem. Phys.* **129**, 224510 (2008).
- [35] J.-S. Lee, R.R. Regatte, A. Jerschow, *J. Magn. Reson.* **200** 126 (2009).
- [36] J.-S. Lee, R.R. Regatte, A. Jerschow, *J. Chem. Phys.* **131** 174501 (2009).
- [37] N. Khaneja, *Phys. Rev. A* **76**, 032326 (2007).
- [38] I.I. Maximov, Z. Tošner, and N.C. Nielsen, *J. Chem. Phys.* **128**, 184505 (2008).
- [39] J.S. Hodges, J.C. Yang, C. Ramanathan, and D.G. Cory, *Phys. Rev. A* **78**, 010303(R) (2008).
- [40] N. Pomplun, B. Heitmann, N. Khaneja, and S.J. Glaser, *Appl. Magn. Reson.* **34** 331 (2008).
- [41] C. Altafini, *J. Math. Phys.* **43**, 2051 (2002).
- [42] C. Altafini, *J. Math. Phys.* **44**, 2357 (2003).
- [43] Y. Maday and G. Turinici, *Int. J. Quantum Chem.* **93**, 223 (2003).
- [44] Y. Maday, J. Salomon, and G. Turinici, *Num. Math.* **103**, 323 (2006).
- [45] G. Dirr, U. Helmke, K. Hüper, M. Kleinsteuber, and Y. Liu, *J. Global Optim.* **35**, 443 (2006).
- [46] K. Ito and K. Kunisch, *SIAM J. Control Optim.* **46**, 274 (2007).
- [47] D. D'Alessandro, *Introduction to Quantum Control and Dynamics*, Chapman & Hall/CRC, 2007.
- [48] M. Bak, J. T. Rasmussen, and N. C. Nielsen, *J. Magn. Reson.* **147**, 296 (2000).
- [49] T. Vosegaard, A. Malmendal, and N. C. Nielsen, *Chem. Monthly* **133**, 1555 (2002).
- [50] M. Lapert, R. Tehini, G. Turinici and D. Sugny, *Phys. Rev. A* **79**, 063411(R) (2009).
- [51] U. Haeberlen and J. S. Waugh, *Phys. Rev.* **175**, 453 (1968).
- [52] M. Hohwy and N. C. Nielsen, *J. Chem. Phys.* **109**, 3780 (1998).
- [53] W. H. Press, S. A. Teukolsky, W. T. Vetterling, and B. P. Flannery, *Numerical Recipes 3rd Edition: The Art of Scientific Computing*, Cambridge University Press, Cambridge, 2007.



- [54] N. C. Nielsen, H. Thøgersen, and O. W. Sørensen, *J. Am. Chem. Soc.* **117**, 11365-11366 (1995).
- [55] N. C. Nielsen, H. Thøgersen, and O. W. Sørensen, *J. Chem. Phys.* **105**, 3962-3968 (1996).
- [56] A. Meissner, J. Ø. Duus, and O. W. Sørensen, *J. Biomol. NMR* **10**, 89 (1997).
- [57] M. Sattler, J. Schleucher, O. Schedletsky, S. J. Glaser, C. Griesinger, N. C. Nielsen, and O. W. Sørensen, *J. Magn. Reson. Ser. A* **119**, 171-179 (1996).
- [58] J. Stoustrup, O. Schedletsky, S. J. Glaser, C. Griesinger, N. C. Nielsen, and O. W. Sørensen, *Phys. Rev. Lett.* **74**, 2921-2924 (1995).
- [59] S. J. Glaser, T. Schulte-Herbrüggen, M. Sieveking, O. Schedletsky, N. C. Nielsen, O. W. Sørensen, and C. Griesinger, *Science* **280**, 421-424 (1998).
- [60] T. Vosegaard, C. Kehlet, N. Khaneja, S. J. Glaser, and N. C. Nielsen, *J. Am. Chem. Soc.* **127**, 13768 (2005).
- [61] E. M. Shapiro, A. Borthakur, A. Gougoutas, and R. Reddy, *Magn. Reson. Med.* **47** 284 (1999).
- [62] MATLAB R2007b, MathWorks ®USA.
- [63] See EPAPS Document No. xxxxxxxx for rf amplitudes and phases of optimal control sequences and MATLAB scripts for the optimal control design of these. For information on EPAPS, see <http://www.aip.org/pubservs/epaps.html>.

## VII. FIGURE CAPTIONS

Fig. 1. (Color online) Pulse sequences for spin-state- and coherence-order-selective  $S^+ \rightarrow I^- S^\alpha$  coherence transfer in a  $J$ -coupled ( $J=140$  Hz) heteronuclear two-spin system designed using optimal control based on the GRAPE algorithm (first row), the original monotonic Krotov-based algorithm (second row), and the latter combined with frequency-truncation smoothing (third row). The red and green lines correspond to  $x$ - and  $y$ -phase rf control fields for the spins  $I$  (left column) and  $S$  (right column), respectively.

Fig. 2. (Color online) Representative pulse sequences obtained throughout the optimization in Fig. 1, illustrating the gradual adoption of the pulse sequence to provide optimum  $S^+ \rightarrow I^- S^\alpha$  coherence transfer with modest rf-power consumption and smooth rf variation. The red and green lines correspond to  $x$ - and  $y$ -phase control fields for spin  $I$  while blue and pink lines represent  $x$ - and  $y$ -phases of the  $S$ -spin control fields.

Fig. 3. (Color online) The dependence of the functional  $J(\omega)$ , the efficiency  $\phi_2$ , and the running cost (penalty) throughout the iteration steps of a smoothing monotonic Krotov-based optimal control design of the pulse sequence for  $S^+ \rightarrow I^- S^\alpha$  coherence transfer, shown and analysed in Figs. 1 and 2. The red curve represents the functional  $J(\omega)$  (defined by Eqs. (4) and (16); for transparency, we have subtracted the correction terms in Eq. (16) which otherwise would add a constant contribution to the functional in all points), the green the efficiency  $\phi_2$ , and blue the penalty cost (see text). All ordinates have been scaled by a factor  $Tr\{CC^\dagger\}$ .

Fig. 4. (Color online) Simulated  $^{23}\text{Na}$  NMR spectra of sodium with a residual quadrupole coupling frequency of  $\omega_Q/2\pi = 60$  Hz excited using a standard  $90^\circ$  hard pulse (red line), the optimal control pulse sequence in Fig. 5A designed to excite exclusively the central transition (green line), and the pulse sequence in Fig. 5B designed to excite the satellite transitions only (blue line).

Fig. 5. (Color online) Optimal control pulse sequences for  $^{23}\text{Na}$  MRI, which for the case of a residual quadrupole coupling of 60 Hz offer selective and enhanced excitation of the central transition (**A**) or excitation of the satellite

transition while suppressing the central peak of the  $^{23}\text{Na}$  NMR/MRI spectrum **(B)**. The red curve represents  $x$ -phase control fields while the green curve represents  $y$ -phase controls. The length of the pulse sequences are 12.5 ms.

Fig. 6. (Color online) Optimal control pulse sequence for excitation of the central peak of the quadrupole spectrum of  $^{23}\text{Na}$  **(A)** (parameters as described in relation to Fig. 4) obtained using the GRAPE algorithm and **(B)** the original Krotov based algorithm. The red and green curves represent  $x$ - and  $y$ -phase control fields. The length of pulse sequences in both cases is 12.5ms.

Fig. 7. (Color online) (a) Excitation profile (normalized) for the central transition as function of the quadrupole coupling frequency for a pulse sequence optimized using our smooth variant of the Krotov algorithm and specifying "broadband" excitation for a range of quadrupole coupling frequencies in proximity of 60 Hz. **(b)** The length of the pulse sequence is 12.5 ms, the RMS average rf power is 170 Hz, and the average transfer efficiency in the range of quadrupolar couplings between 40 and 80 Hz is 1.89 (corresponding to 95 % of the theoretical maximum).

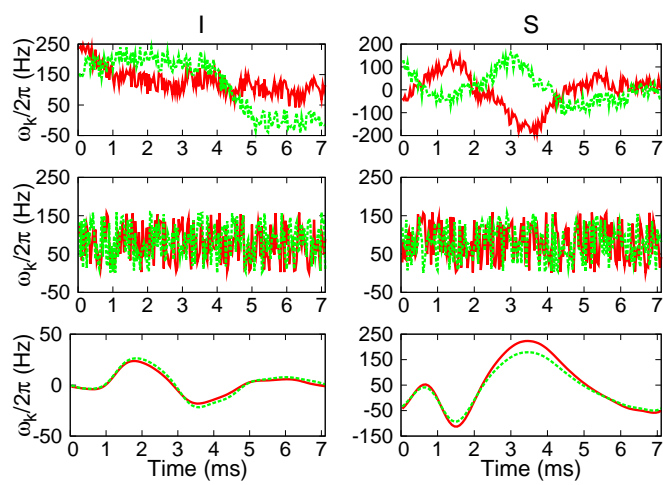


FIG. 1.

Figure 1:

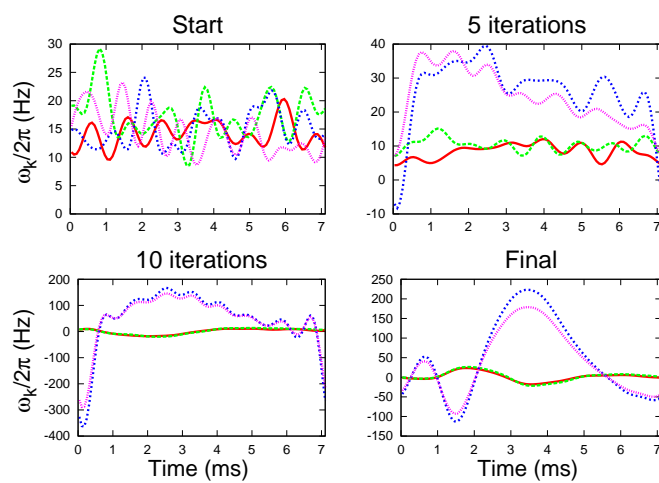


FIG. 2.

Figure 2:

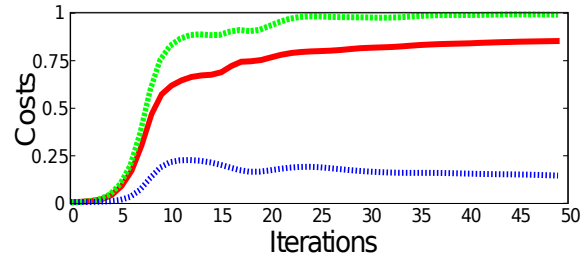


FIG. 3.

Figure 3:

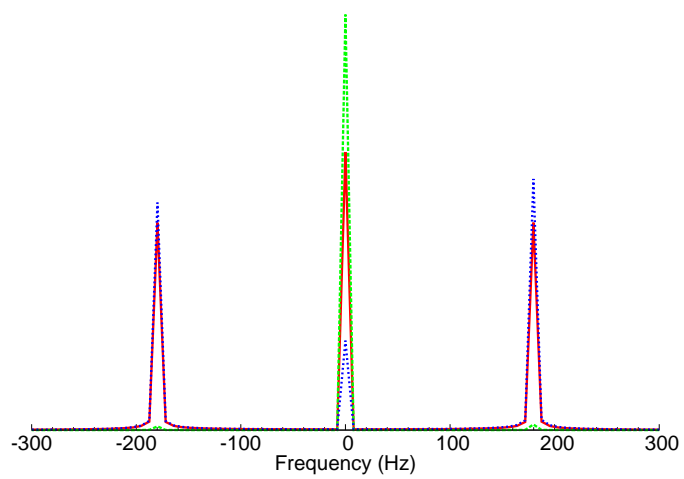


FIG. 4.

Figure 4:

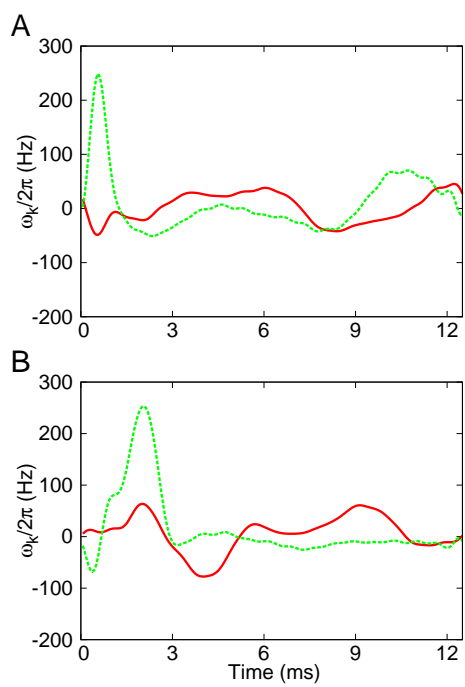


FIG. 5.

Figure 5:



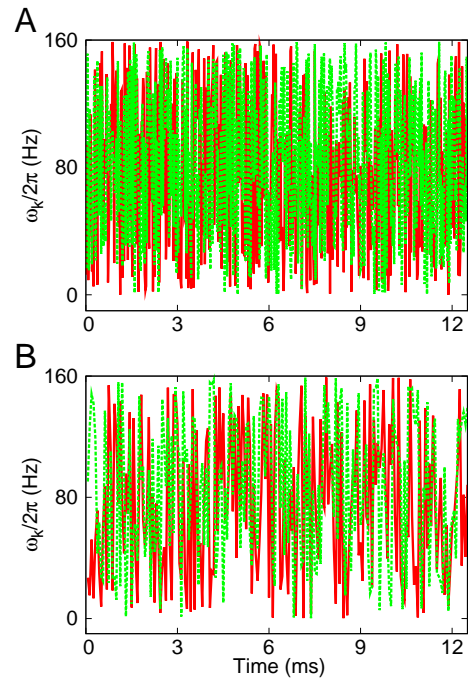


FIG. 6.

Figure 6:

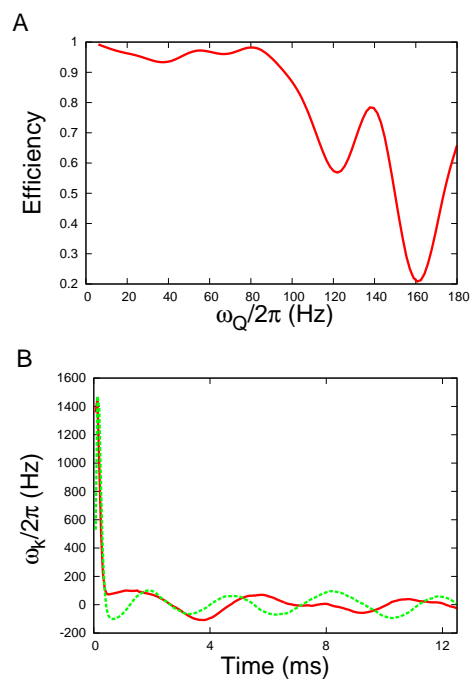


FIG. 7.

Figure 7: